Scalable Method for the Reductive Dissolution, Purification, and Separation of Single-Walled Carbon Nanotubes

Siân Fogden,[†] Christopher A. Howard,[‡] Richard K. Heenan,[§] Neal T. Skipper,[‡,*] and Milo S. P. Shaffer[†,*]

[†]London Centre for Nanotechnology, Department of Chemistry, Imperial College London, South Kensington Campus, London, SW7 2AZ, U.K., [‡]London Centre for Nanotechnology, Department of Physics and Astronomy, University College London, Gower Street, London, WC1E 6BT, U.K., and [§]ISIS, STFC Rutherford Appleton Laboratory, Chilton, Didcot, OX11 0QX, U.K.

ABSTRACT As synthesized, bulk single-walled carbon nanotube (SWNT) samples are typically highly agglomerated and heterogeneous. However, their most promising applications require the isolation of individualized, purified nanotubes, often with specific optoelectronic characteristics. A wide range of dispersion and separation techniques have been developed, but the use of sonication or ultracentrifugation imposes severe limits on scalability and may introduce damage. Here, we demonstrate a new, intrinsically scalable method for SWNT dispersion and separation, using reductive treatment in sodium metal-ammonia solutions, optionally followed by selective dissolution in a polar aprotic organic solvent. *In situ* small-angle neutron scattering demonstrates the presence of dissolved, unbundled SWNTs in solution, at concentrations reaching at least 2 mg/mL; the ability to isolate individual nanotubes is confirmed by atomic force microscopy. Spectroscopy data suggest that the soluble fraction contains predominately large metallic nanotubes; a potential new mechanism for nanotube separation is proposed. In addition, the G/D ratios observed during the dissolution sequence, as a function of metal: carbon ratio, demonstrate a new purification method for removing carbonaceous impurities from pristine SWNTs, which avoids traditional, damaging, competitive oxidation reactions.

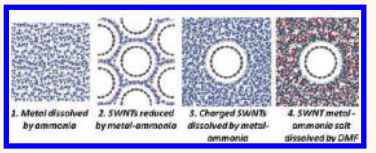

KEYWORDS: single-walled carbon nanotubes · nanotubide · reductive dissolution · purification · separation

The extraordinary electronic and optical properties of single walled carbon nanotubes (SWNTs) are determined by their structure; SWNTs are either metallic or semiconducting, depending on their diameter and chirality.[1] Many valuable applications in, for example, transparent conductors,[2] solar cells,[3] biosensors,[4] and nanoelectronics[5] require individualized carbon nanotubes of specific electronic character and high purity. For this reason, there has been a concerted effort to provide methods for separation of individual SWNT species. Despite recent progress in selective synthesis, current techniques still produce heterogeneous samples containing SWNTs of varying geometry and electronic character, as well as other carbonaceous contaminants.[6,7] Postproduction separation of metallic and semiconducting SWNTs follows various strategies based on physical (dielectrophoresis,[8] density gradient ultracentrifugation,[9] gel electrophoresis,[10] and chromatography[11]) and chemical (diazonium salts,[12] ozonolysis,[13] diporphyrin,[14] bromine,[15] amine,[16] and pyrene functionalization[17]) means. All of these methods suffer from problems with scalability, effectiveness, and often dissolution sensitivity. Additionally, chemical functionalization methods are limited by the inherent potential to damage the outstanding electronic, optical, and mechanical properties of interest.[18]

While some larger volume separation techniques have been demonstrated,[8,10,19] the initial dispersion step remains limiting. SWNTs form bundles due to strong van der Waals interactions; so, before any fractionation attempt, the SWNTs must be individualized by high-power sonication in organic solvent or, most commonly, aqueous surfactant solution.[8,10,16] Sonication is known to damage the SWNT structure by both shortening and functionalization.[20] The resulting solutions are intrinsically low concentration and almost always require ultracentrifugation for the complete removal of small bundles,[21] greatly limiting the scalability of these methods. The only means to dissolve SWNTs without sonication rely on charging effects, either protonation in superacids[22] or reduction (indirectly) with alkali metals.[23] Penicaud *et al.* showed that SWNTs can be reduced with sodium naphthalene in THF, leading to spontaneous dissolution in

* E-mail:
n.skipper@ucl.ac.uk;
m.shaffer@imperial.ac.uk.

Received for review June 24, 2011
and accepted December 14, 2011.

Published online December 29, 2011
10.1021/nn2041494

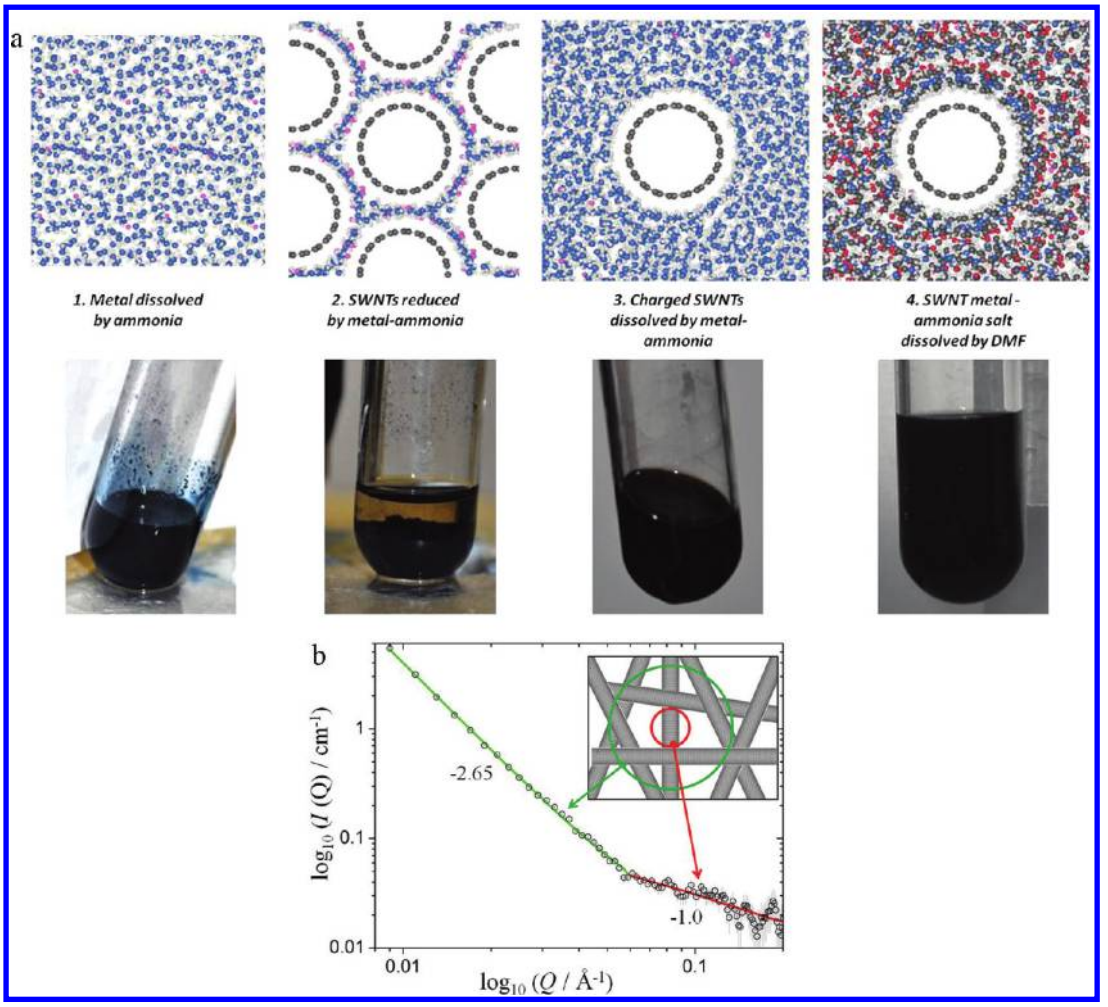

Figure 1. Liquid ammonia reduction of ARC SWNTs. (a) Process scheme for the reduction, solvation, and subsequent dissolution in sodium-ammonia, illustrated by atomistic models (Na ions in pink) and photographs of relevant phases (M:C 1:20). (b) SANS pattern from the spontaneously dissolved SWNTs (M:C 1:24) in sodium-ammonia ($Na:ND_3$). The red and green lines show power-law best fits, giving exponents of −1.0 and −2.65, as marked. The inset shows a schematic of the corresponding nanotube mesh and associated length scales.

various aprotic polar solvents, and the identification of individual SWNTs in subsequent, dry AFM.[23] However, no selective electronic separation of nanotubes or impurities has been reported using either approach; in Penicaud's method, the sodium naphthalide remains in the system as a contaminant.

Using liquid ammonia as the charging solvent avoids this contamination problem, since the ammonia can be simply removed by evaporation. When an alkali metal is dissolved in liquid ammonia, solvated electrons are formed (seen as an intense blue color within the solution[24]); these solvated electrons can then be transferred to the SWNTs.[25−28] The resulting reduced SWNTs have been reported previously to disperse more easily with "continued stirring" in liquid ammonia,[29] with AFM evidence of individual SWNTs after chemical grafting reactions.[26] The mechanism for this reactive debundling is still under some debate, with intertube repulsions and alkali metal intercalation most commonly suggested.[26,29] Using ammonia as a solvent, Wunderlich *et al*. suggested that metallic and small-diameter SWNTs are preferentially chemically functionalized due to strain and charging effects,[28,30] although no fractionation was undertaken.

In this work, we use *in situ* small-angle neutron scattering (SANS) to demonstrate that SWNTs can indeed be unbundled to give individual tubes in solution by reductive charging in ammonia. This process requires control of the metal:carbon (M:C) ratio, to much lower values (approximately 1:10) than typical in the literature (>1:1), but does not inherently involve covalent functionalization of the tubes. Transfer of these reduced nanotubes, as a dry powder, to an organic solvent allows for straightforward fractionation of the spontaneously dissolved material, which was found to contain predominantly larger metallic SWNTs and impurities.

RESULTS AND DISCUSSION

SWNT Reduction in Liquid Ammonia. The initial treatment of SWNTs in liquid sodium metal ammonia solution is a

key step in the separation. Here, unlike in the THF/napthalide route, the electrons are directly solvated, and no secondary charge transfer agent is required. When liquid ammonia is condensed onto a mixture of ARC SWNT and alkali metal, the initially colorless liquid ammonia turns blue, due to the dissolution of the metal and the concomitant 1s−2p transition of solvated electrons.[24] In the absence of stirring, the SWNT powder swells, and gradually over the course of approximately two hours, the solution changes from blue to clear to black, as the nanotubes accept the solvated electrons, spontaneously debundle, and dissolve into the liquid ammonia (reaction scheme Figure 1a).

The structure of the SWNTs in liquid sodium-ammonia was characterized by small-angle neutron scattering. SANS is a powerful technique for probing the structure of nanoparticles in solution,[31−34] and specifically can be used to determine whether the SWNTs are present as isolated species or as bundles or clusters.[33] In the dilute regime, the SANS intensity is $I(Q) \propto Q^{-D}$, where $Q = 4\pi \sin(\theta)/\lambda$ is the magnitude of the scattering wavevector and D is the fractal dimension of the scattering objects. Thus a plot of $\log_{10} I(Q)$ against $\log_{10} Q$ will yield a straight line of gradient $-D$. Fully dispersed rod-like objects such as individual SWNTs will have a dimensionality $D \approx 1$, and their expected SANS signal is therefore $I(Q) \propto Q^{-1}$. Heterogeneous dispersions of SWNTs, consisting of agglomerates and bundles (effectively rod networks), will exhibit a larger fractal dimension,[31,32,34] typically in the range $D \approx 2$ to 4.

SANS data from a solution of ARC SWNTs dissolved in sodium-deuteroammonia (ND_3) solution show two clear scattering regimes (Figure 1b). At higher Q-values, up to at least $Q \approx 0.2$ Å^{-1}, there is a Q^{-1} dependence that can be quantitatively fitted by a model containing cylindrical rods of diameter 15−20 Å (see Methods). This dimension is entirely consistent with the value of ∼14 Å reported for the diameter of ARC-SWNTs, since each tube will be surrounded by a dense ordered shell of solvent (see atomistic simulation, Figure 1a). This solvation behavior is expected to be similar to that deduced from neutron diffraction studies of C_{60} anions dissolved in ammonia, where isotopic labeling and the intrinsic monodispersity allowed the solvent structure to be explicitly determined.[35] However, we note that since SANS intensity typically scales as the particle volume squared, scattering from any fullerene species (as measured previously) will fall below the sensitivity of our data, in the current case (see SI Figure S1). Conversely, if the dissolved material consisted of a significant fraction of graphitic nanoparticles that are known to occur in arc soots,[36] they would contribute noticeably to the SANS signal, giving a higher dimensionality; thus, a large fraction of dissolved nanoparticles is not consistent with the Q^{-1} dependence (rods) observed.

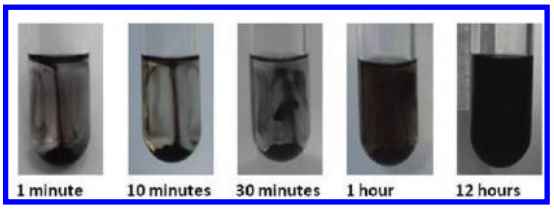

Figure 2. Photographs showing the spontaneous dissolution of 10 mg of ARC nanotubide salt (M:C 1:20) into 10 cm^3 dry DMF.

The second regime in Figure 1b has $Q^{-2.65}$ behavior, with the crossover indicating the smallest size of the larger scatterers. For concentrated solutions of SWNTs, effectively, there is a mesh formed[34] (see Figure 1b inset), which gives rise to this higher power-law scattering at lower Q. Previously, a $Q^{-2.5}$ power law has been proposed in this regime,[34] based on infinitely thin rods; the slightly higher value of the fractal dimension (2.65) obtained here, directly from a free fit, is consistent with rods of finite thickness and is identical to that obtained from detailed analysis of SEM and TEM images of carbon nanotube films.[37] From the fitted SANS data, it is possible to deduce that the approximate concentration of individual SWNTs in solution is in the range 2−12 mg/mL (up to 0.75% SWNT by volume; see Methods). This range is consistent with the crossover in Figure 1b, found at $Q \approx 0.055$ Å^{-1}, equivalent to a mesh size $\xi \approx 115$ Å. Hough *et al.*[33] reported that in sodium dodecylbenzenesulfonate-stabilized aqueous suspension, $\xi = 150$ Å corresponds to a 0.75 wt % SWNT solution.

DMF Addition to the Nanotubide Salt−SWNT Separation. Following the removal of the liquid ammonia, a dry powder of sodium "nanotubide" is formed (where "nanotubide" is the proposed term for a pure nanotube anion). On the addition of dry DMF (Figure 2), the ARC nanotubide swells and a fraction (approximately 40 wt %) of the SWNTs spontaneously dissolves. It is worth emphasizing that no stirring and, more importantly, no ultrasound were used at any stage of the process. As in the work of Penicaud,[23] this spontaneous dissolution is presumably driven by the solvation of the cations, leading to repulsion between the solvated nanotubide anions and the formation of an electrostatically stabilized colloid (or polyelectrolyte molecule). The use of oxygen and water-free solvent is essential to avoid quenching the charge through the formation of sodium (hydr)oxide. The solution in organic solvent allows straightforward fractionation via cannula, although reliable discrimination of the phases becomes difficult at higher concentration. The maximum measurable concentration was found to be 2 mg/mL, although, again, this value should be considered a lower bound.

Sodium nanotubide based on CoMoCAT SWNTs, produced by the same ammonia process, also spontaneously dissolves in DMF (dissolved yield 14 wt %) with a similar minimum solubility (2 mg/mL). SEM

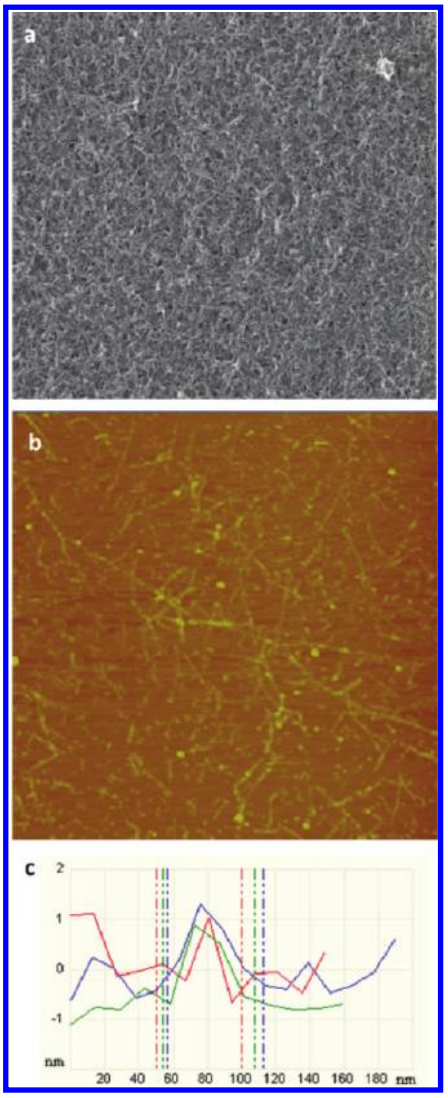

Figure 3. Microscopy images of CoMoCAT SWNTs spontaneously dissolved into dry DMF (M:C 1:10). (a) SEM X- and Y-scale 2 μm. (b) AFM X- and Y-scale 3 μm, Z-scale 0−45 nm. (c) Height section from AFM images showing the height of three SWNTs in different areas of the sample.

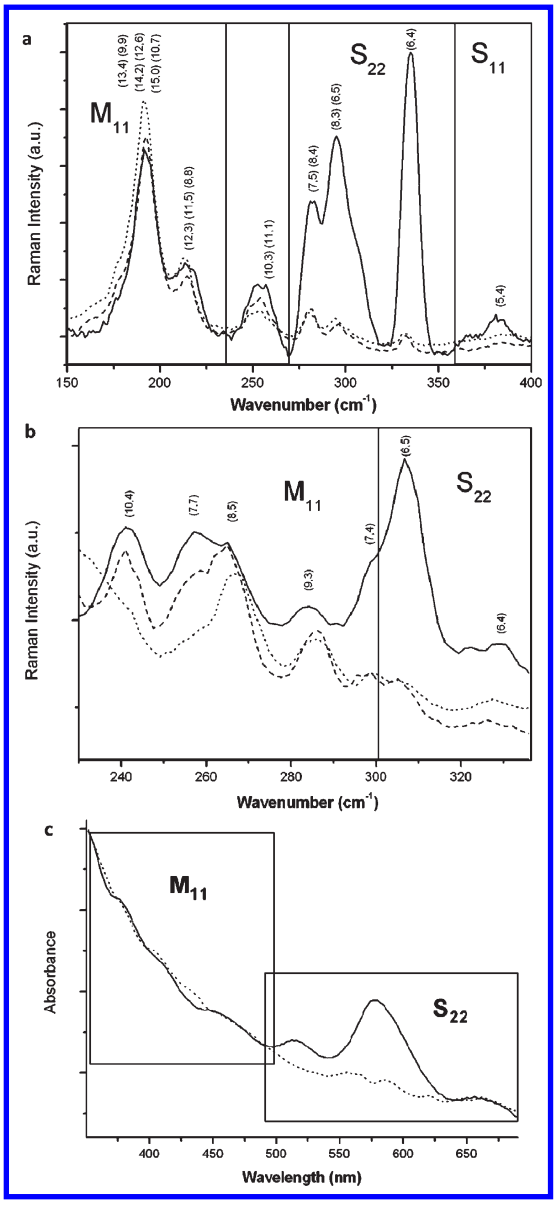

Figure 4. Optical characterization of SWNT fraction spontaneously dissolved into DMF at the M:C ratio 1:10. (a) Red (633 nm) RBM Raman spectra of as-received CoMoCAT SWNTs (solid line), the spontaneously dissolved CoMoCAT fraction (dashed line), and the spontaneously dissolved CoMoCAT fraction following vacuum annealing (dotted line). The regions corresponding to metallic or semiconducting transitions are marked. (b) Green (532 nm) RBM Raman spectra of as-received CoMoCAT SWNTs (solid line), the spontaneously dissolved CoMoCAT fraction (dashed line), and the spontaneously dissolved CoMoCAT fraction followed by vacuum annealing (dotted line). (c) UV/vis spectra of as-received CoMoCAT SWNTs (solid line) and spontaneously dissolved fraction (dotted line).

(Figure 3a) and AFM (Figure 3b and c) confirm that the dissolved fraction consists predominantly of nanotubes; the AFM, in particular, shows that the dissolved species are individualized SWNTs with diameters 1.0−1.5 nm.

The relative metallicity of the SWNT fractions was estimated from the positions of the radial breathing modes (RBMs) observed using Raman spectroscopy; the SWNT diameters[38] ($\omega_{rbm} = 218.7/d + 15.3$) were correlated with the diameter-dependent transition energies between the Van Hove singularities using the Kataura plot,[39] to assign bands to particular electronic type. While the assessment is highly diameter dependent, selecting a probe wavelength in resonance with both metallic and semiconducting species provides an effective means to monitor relative changes with the sample. Both metallic and semiconducting species within the as-supplied CoMoCAT SWNTs conveniently couple to the red (633 nm) and green (532 nm) lasers available. Excitation using the red laser shows seven distinct peaks; using previously established methods,[38,39] the tube diameters can be calculated and the peaks indexed (Figure 4a). The intensity of the tube peaks is only comparative, not absolute, as

the efficiency of resonant energy transfer varies;[40] it is known, for example, that (6, 5) tubes dominate CoMoCAT samples, although they couple weakly to the red laser. In the spontaneous dissolution process, the intensity of the peaks correlating to the semiconducting SWNTs decreases strongly, disappearing almost entirely. The Raman data also suggest a diameter effect, with preferential dissolution of larger metallic nanotubes. Although apparent shifts in RBM distributions have been reported on debundling,[41] due to changes in interband transition energies, no shifts were observed in the metallic region of the spectra, indicating any such effects are minimal; most likely, SWNTs rebundle during charge quenching in suspension before sampling for Raman measurements. Related overall trends, dependent on both electronic character and size, have been observed during the deliberate covalent functionalization of charged SWNTs;[28,30] in the current case, no explicit reagents were added; the possibility of significant, accidental, selective functionalization is addressed by experiments discussed in the Mechanism section below. The green Raman laser line (Figure 4b) shows a similar relative decrease in intensity of the semiconducting peaks in the spontaneously dissolved fraction, both before and after vacuum annealing. The Raman data for the original salt and subsequent dissolved fractions are homogeneous across the sample; the spectra for the remaining undissolved fractions are more heterogeneous, presumably reflecting the difficultly in isolating the sediment from the last drops of dispersion and the potential for otherwise soluble nanotubes to remain trapped due to entanglements or amorphous debris.

UV/vis spectroscopy has the potential to provide complementary evidence of the degree of separation. Indeed, a reduction in the size of the semiconducting peak is observed following the dissolution in the DMF, Figure 4c. The first Van Hove transition of the metallic species can be seen in the 350−500 nm range, although the low intensity of the peaks in the as-received sample parallels the small fraction of metallic SWNTs present. The second Van Hove transitions of the semiconducting SWNTs fall in the 480−700 nm range. In this range, the largest peak at 560 nm relates to the (6,5) SWNT, which is known[40] to be the dominant tube in this CoMoCAT material. Despite extensive attempts using different approaches, the signal from the dissolved fraction remains weak; the result may relate to an increased concentration of impurities, as indicated by the Raman studies of the "D-band" discussed below, limited functionalization during quenching, and/or the difficulty in redispersing dense bundles formed on drying individualized SWNTs from solution. Note that spectra cannot be obtained from the spontaneously dissolved SWNTs due to the bleaching of optical transitions associated with charging or doping of the Van Hove features.[42]

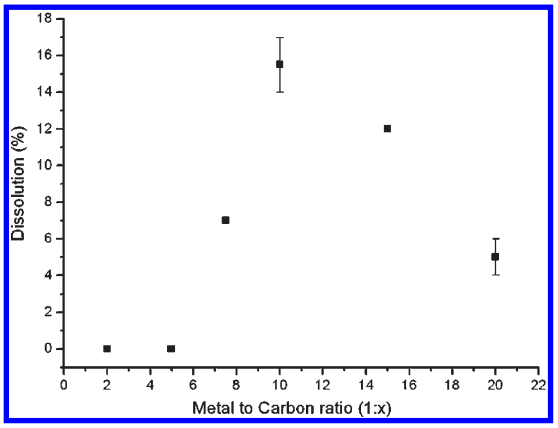

Figure 5. Mass fraction dissolved spontaneously, following metal-ammonia and DMF treatment; 20 mg of CoMoCAT SWNTs was used in each experiment.

Figure 6. Spontaneously dissolved fraction from a 1:10 metal to carbon ratio reduction stored in inert atmosphere for 6 months, 1 min and 12 h after exposure to air.

Raman spectroscopy provides a semiquantitative indication of purity or degree of functionalization by comparing the relative intensity of the defect band (D-band) at ~1350 cm^{-1} and the graphite band (G-band) at ~1580 cm^{-1}; although the details are complex, increasing D-band intensity is usually correlated with either the presence of other contaminating carbons or damage to the nanotube framework. The initial G/D ratio of around 11 does not change following the ammonia treatment even after air-exposure, consistent with a lack of significant covalent functionalization (see SI Figure S2 for a summary plot of the G/D ratios obtained). Similarly, energy-dispersive X-ray spectroscopy showed no evidence of nitrogen incorporation in any of the liquid ammonia- or DMF-treated samples. However, the G/D ratio drops to 7 in the spontaneously dissolved fraction, while increasing to 18 in the undissolved material. This divergent trend suggests that carbonaceous impurities (or short/defect SWNTs) are preferentially dissolved with or before the metallic fraction, although the dissolved material is predominantly SWNTs at our standard M:C ratios, as discussed above.

This hypothesis was confirmed using a much lower M:C ratio (1:100); in this case, only a small mass fraction dissolved spontaneously, giving a very low G/D ratio around unity, leaving the bulk material as a residue, again with an improved G/D of 18. Thus, the overall method can be used for purification as well as dispersion and separation. SEMs of the remaining, undissolved material (see SI Figure S2) show well-defined, apparently cleaner, SWNTs.

Yield and Scalability. The yield (Figure 5) of spontaneously dissolved CoMoCAT SWNTs in DMF depends strongly on metal to carbon ratio (M:C). The optimum atomic ratio of 1:10 M:C consistently corresponds to a maximum dissolved yield of 15 ± 1 wt % of the original sample. Further washings with fresh solvent do not dissolve additional material; the remaining, undissolved SWNTs are either inappropriately charged or physically trapped by entanglements or insoluble amorphous carbon. At lower metal loadings, the yield declines due to insufficient charge for electrostatic repulsion between the nanotubes and/or charge-driven solvation. At higher loadings, the yield declines due to excessive sodium ion concentration, leading to "salting" out, as the Debye length declines. A similar optimum (1:12) was identified previously for the dissolution of C_{60}^{5-} in metal-ammonia solutions.[43] It is worth noting that the great majority of literature studies of nanotubes in ammonia use a metal to carbon ratio of 1:1 or higher, which is not expected to yield individualized nanotubes, for either debundled functionalization or separation.

The reaction was found to be scalable at the optimum 1:10 M:C ratio. On increasing the initial quantity of SWNTs from 20 mg to 50 mg and 100 mg, the reaction proceeded in the same manner, yielding 14 wt % and 17 wt % of spontaneously dissolved nanotubes, respectively. Similar Raman spectra were obtained for the spontaneously dissolved component in all cases (see SI Figure S3).

Mechanism. The dissolution process is driven by the solvation of the sodium cations, electrostatic repulsion between the nanotubes, and the relatively favorable enthalpic interactions of nanotubes with both amides[44] and ammonia, particularly when charged.[43] The dominant importance of the charged state is clearly demonstrated (Figure 6) by the long-term stability of the DMF dispersions in the absence of air (>6 months), but rapid agglomeration on quenching the charge with air (minutes). While the use of DMSO as a solvent for nanotubide has been reported to lead to covalent modification and permanent modification of solubility,[45] the sensitivity to air in the current case strongly suggests that the solution stability is due to electrostatic repulsion between charged nanotubes rather than any permanent chemical reaction with the ammonia or DMF. Exposure to oxygen (in air) is reported to quench the charge on reduced SWNTs without oxidative addition.[46,47] Whilst adventitious moisture may have an influence, a low level of functionalization is implied in this study by the G/D Raman data above and, specifically, by vacuum-annealing the spontaneously dissolved sample at 500 °C, $<10^{-6}$ mbar, for 24 h. This process is often used to remove unwanted functional groups and (partially) restore original optoelectronic properties;[48] however, the Raman spectra of the dissolved SWNT fraction was unchanged by this treatment. The spontaneous nature of the dissolution confirms that it is thermodynamically favored and, therefore, likely to give rise to individualized SWNTs. Previous estimates for the Bjerrum length,[23] the minimum separation of surface charge before counterion condensation becomes thermodynamically favorable, suggest that a 1:50 M:C ratio should be optimal for nanotubes; very recent refinements have identified a slightly lower optimum ratio (<1:20) and provide a detailed discussion of the thermodynamics of the electrostatic stabilization.[49] However, these estimates rely entirely on the dielectric constant of the solvent; in reality, the dielectric constant of the nanotube will make a major contribution, particularly for metallic tubes. Qualitatively, the higher dielectric constant of the metallic SWNTs should reduce the effective Bjerrum length, increasing the maximum surface charge that can be accommodated before "salting" out occurs and raising the electrostatic stability of the dispersed state relative to the semiconducting SWNTs; larger diameter nanotubes are also expected to have higher dielectric constants.[50] Detailed calculations require a revision of the traditional theory, beyond the scope of this study, but would be of great interest. While this hypothesis for the size and electronic selectivity of the dissolution process appears plausible, the variation of dielectric constant on charging SWNTs is not yet known, and other selective mechanisms may contribute. Intrinsically, different nanotubes have characteristic electron affinities, and thus charge will be partitioned heterogeneously when in contact. While the Fermi level appears to be a function of diameter,[51] metallic nanotubes will always have greater initial electron affinity than semiconducting species, an effect exploited in selective diazonium functionalization reactions and other chemistries.[12] In the present case, however, there is sufficient charge available to saturate at least the first Van Hove singularities, and the distinction between the multiple electron affinities of the various nanotube types is less obvious. Although charge effects clearly dominate, the selective solubilizing interactions of DMF may also play a role.[52]

CONCLUSIONS

Liquid ammonia has been shown to be an excellent medium for creating powders of alkali metal nanotubide salts, avoiding the need of any additional charge transfer species through the intrinsic electron-solvating power

of the ammonia. These salts can be conveniently dissolved in dry amide solvents to form solutions of individual charged SWNTs that can be readily handled. The dissolution of a variety of as-synthesized SWNTs occurs without any sonication, stirring, or chemical functionalization, as long as the metal:carbon ratio is carefully controlled (to lower levels than typical in the literature); the high aspect ratios and characteristics of pristine SWNT can thus be retained. The process was found to work similarly for HiPco SWNTs (see SI Figure S4). At very low metal contents, carbonaceous impurities are selectively removed, providing a nondestructive means of SWNT purification. At high metal contents, the spontaneously dissolved fraction appears to consist mainly of larger metallic SWNTs, suggesting the possibility of straightforward separations by electronic character without use of ultrasound or centrifugation. The exact nature of the separated samples could be clarified by specialists in individual SWNT methods; while laborious, measurements of individual properties, particularly transport characteristics, are highly relevant to application. This new separation process has been shown to scale consistently to the 100 mg level, and there is no intrinsic reason that it could not provide larger scale separation and/or purification of SWNTs in the future (see SI Figure S3). The availability of large quantities of individualized, purified, undamaged SWNTs will enable further fundamental studies of SWNT phenomena and a wide range of applications.

METHODS

Preparation of Separated SWNTs. SWNTs were purchased from Carbon Solutions (ARC grown) and Southwestern Nanotechnologies (CoMoCat, CVD grown) and used as received. In a typical experiment, 20 mg of SWNTs was accurately weighed in a high-purity argon glovebox and placed in a specially designed glass reaction tube, which was then outgassed at 400 °C for 48 h at $<10^{-6}$ mbar. A 2 mg amount of sodium was accurately weighed and transferred to the reaction tube, which was cooled at −50 °C in either a propanol/dry ice bath or in propanol cooled using a chiller unit. A 0.12 mol sample of ammonia (Aldrich at 99.9% purity) was then condensed onto the reaction mixture, and after approximately 2 h the ammonia was removed from the mixture by cryo-pumping. With the complete exclusion of air, dry DMF (Aldrich, anhydrous 99.8%) was then added to the SWNT powder using standard Schlenk line techniques, after which a fraction could be seen to dissolve spontaneously. Samples were vacuum annealed at 500 °C under a vacuum of $<10^{-6}$ mbar for 24 h. In some experiments, the mass of SWNTs and/or metal was varied to control the metal to carbon ratio or absolute reaction scale.

Raman Spectra Measurements. Raman spectra of dry samples were collected with a LabRam Infinity Raman instrument using red (633 nm) and green (532 nm) lasers.

Optical Absorbance Measurements. UV/vis/near-IR spectra were collected using a Perkin-Elmer Lambda 950 following the dispersion of the SWNT sample in D_2O and sodium cholate using 30 W sonication for 5 min and high-speed centrifugation.

Atomic Force Microscopy Images. AFM images were obtained using a Nanoscope IV Digital Instruments AFM in tapping mode, using samples prepared by spin-coating the spontaneously dissolved fraction onto a mica substrate.

Small-Angle Neutron Scattering Measurements. SANS data were collected on the LOQ beamline at the ISIS pulsed neutron source, using neutrons of wavelengths 2.2 to 10 Å recorded by time-of-flight at a 64 cm square position sensitive detector, 4.19 m from the sample. Samples were contained in a 2 mm path fused silica cell inside an evacuated closed cycle He refrigerator (CCR). The solutions were made *in situ* on the beamline by condenstation of 2 cm^{-3} deuterammonia (ND_3) onto excess (20 mg) ARC SWNTs and sodium metal at a carbon to metal ratio of 1:24. The 12 mm diameter neutron beam sampled only the upper half of the cell, containing spontaneously dissolved material. Background subtractions, which were dominated by scattering from the cell and CCR vacuum tails, were measured for the same cell filled with ND_3. Data were corrected for wavelength-dependent sample transmissions and detector efficiencies and then scaled to absolute scattering cross-section, $I(Q)$, by comparison to data from a partially deuterated polystyrene standard.

SANS data were fitted using the program Fish,[53] which employs a standard iterative linear least-squares method involving computation of first derivatives of each calculated data point with respect to each parameter in the model. The best fit shown in Figure 1b was obtained by using a model in which the data were fitted in two regimes.

The low-Q region ($Q < 0.055$ Å^{-1}) was fitted to a power law:

$$I(Q) = CQ^{-D} + B$$

where C is a constant and B the incoherent background, and the fractal dimension was found to be $D = 2.65$.

The high-Q region ($Q \geq 0.055$ Å^{-1}) was fitted to the expression[53]

$$I(Q) \propto N_p V_p{}^2 \Delta\rho^2 P(Q) + B$$

where N_p is the number concentration of scattering bodies, V_p is the volume of one scattering body, $\Delta\rho$ is the difference in neutron scattering length density between the scattering bodies and the solvent (the so-called "contrast"), B is again the incoherent background, and $P(Q)$ is the form (shape) factor, corresponding to randomly oriented cylindrical rods of effective diameter ~15−20 Å. This model then yields a nanotube concentration of approximately 0.17−0.75 vol % or 2−12 mg/mL, for effective rod diameters of 20 and 15 Å, respectively.

Acknowledgment. The authors thank Ann Terry, Mike Yates, and Andy Church (ISIS Facility) and Emily Milner and Arthur Lovell (UCL) for assistance with the SANS experiments, ISIS for neutron beamtime, Bio-Nano Consulting Ltd. for research support, and the UK's EPSRC and Linde for funding. Initial research support was provided by the EPSRC directly (EP/E501141/1) and through the IRC in Nanotechnology (GR/R45680/01); additional support for this project was provided by Linde North America Inc., through Bio-Nano Consulting Ltd. Associated patent filings have been licensed to Linde North America Inc., where S.F. has recently been employed.

Supporting Information Available: This material is available free of charge *via* the Internet at http://pubs.acs.org.

REFERENCES AND NOTES

1. Meyyappan, M. *Carbon Nanotubes: Science and Applications*; CRC Press, 2005.
2. Cao, Q.; Rogers, J. A. Ultrathin Films of Single-Walled Carbon Nanotubes for Electronics and Sensors: A Review of Fundamental and Applied Aspects. *Adv. Mater.* **2008**, *21*, 29–53.

3. Gabor, N. M.; Zhong, Z. H.; Bosnick, K.; Park, J.; McEuen, P. L. Extremely Efficient Multiple Electron-Hole Pair Generation in Carbon Nanotube Photodiodes. *Science* **2009**, *325*, 1367–1371.
4. Allen, B. L.; Kichambare, P. D.; Star, A. Carbon Nanotube Field-Effect-Transistor-Based Biosensors. *Adv. Mater.* **2007**, *19*, 1439–1451.
5. Burghard, M.; Klauk, H.; Kern, K. Carbon-Based Field-Effect Transistors for Nanoelectronics. *Adv. Mater.* **2009**, *21*, 2586–2600.
6. Lolli, G.; Zhang, L.; Balzano, L.; Sakulchaicharoen, N.; Tan, Y.; Resasco, D. E. Tailoring (n,m) Structure of Single-Walled Carbon Nanotubes by Modifying Reaction Conditions and the Nature of the Support of CoMo Catalysts. *J. Phys. Chem. B* **2006**, *110*, 2108–2115.
7. Li, X. L.; Tu, X.; Zaric, S.; Welsher, K.; Seo, W. S.; Zhao, W.; Dai, H. Selective Synthesis Combined with Chemical Separation of Single-Walled Carbon Nanotubes for Chirality Selection. *J. Am. Chem. Soc.* **2007**, *129*, 15770–15771.
8. Krupke, R.; Hennrich, F.; von Lohneysen, H.; Kappes, M. M. Separation of Metallic from Semiconducting Single-Walled Carbon Nanotubes. *Science* **2003**, *301*, 344–347.
9. Arnold, M. S.; Green, A. A.; Hulvat, J. F.; Stupp, S. I.; Hersam, M. C. Sorting Carbon Nanotubes by Electronic Structure Using Density Differentiation. *Nat. Nanotechnol.* **2006**, *1*, 60–65.
10. Moshammer, K.; Hennrich, F.; Kappes, M. M. Selective Suspension in Aqueous Sodium Dodecyl Sulfate According to Electronic Structure Type Allows Simple Separation of Metallic from Semiconducting Single-Walled Carbon Nanotubes. *Nano Res.* **2009**, *2*, 599–606.
11. Heller, D. A.; Mayrofer, R. M.; Baik, S.; Grinkova, Y. V.; Usrey, M. L.; Strano, M. S. Concomitant Length and Diameter Separation of Single-Walled Carbon Nanotubes. *J. Am. Chem. Soc.* **2004**, *126*, 14567–14573.
12. Strano, M. S.; Dyke, C. A.; Usrey, M. L.; Barone, P. W.; Allen, M. J.; Shan, H.; Kittrell, C.; Hauge, R. H.; Tour, J. M.; Smalley, R. E. Electronic Structure Control of Single-Walled Carbon Nanotube Functionalization. *Science* **2003**, *301*, 1519–1522.
13. Banerjee, S.; Wong, S. S. Demonstration of Diameter-Selective Reactivity in the Sidewall Ozonation of SWNTs by Resonance Raman Spectroscopy. *Nano Lett.* **2004**, *4*, 1445–1450.
14. Peng, X.; Komatsu, N.; Bhatacharya, S.; Shimawaki, T.; Aonuma, S.; Kimura, T.; Osuka, A. Optically Active Single-Walled Carbon Nanotubes. *Nat. Nanotechnol.* **2007**, *2*, 361–365.
15. Chen, Z. H.; Xu, D.; Mao-Hua, D.; Ranchken, C. D.; Hai-Ping, C.; Rinzler, A. G. Bulk Separative Enrichment in Metallic or Semiconducting Single-Walled Carbon Nanotubes. *Nano Lett.* **2003**, *3*, 1245–1249.
16. Maeda, Y.; Kanda, M.; Hashimoto, M.; Hasegawa, T.; Kimura, S.; Lian, Y.; Wakahara, T.; Akasaka, T.; Kazaoui, S.; Minami, N.; *et al*. Dispersion and Separation of Small-Diameter Single-Walled Carbon Nanotubes. *J. Am. Chem. Soc.* **2006**, *128*, 12239–12242.
17. Wang, W.; Fernando, K. A. S.; Lin, Y.; Meziani, M. J.; Cao, L.; Zhang, P.; Kimani, M. M.; Sun, Y.-P. Metallic Single-Walled Carbon Nanotubes for Conductive Nanocomposites. *J. Am. Chem. Soc.* **2008**, *130*, 1415–1419.
18. Zhao, J. J.; Park, H. K.; Han, J.; Lu, J. P. Electronic Properties of Carbon Nanotubes with Covalent Sidewall Functionalization. *J. Phys. Chem. B* **2004**, *108*, 4227–4230.
19. Tanaka, T.; Jin, H.; Miyata, y.; Fujii, S.; Suga, H.; Naitoh, Y.; Minari, T.; Miyadera, T.; Tsukagoshi, K.; Kataura, H. Simple and Scalable Gel-Based Separation of Metallic and Semiconducting Carbon Nanotubes. *Nano Lett.* **2009**, *9*, 1497–1500.
20. Moonoosawmy, K. R.; Kruse, P. To Dope or Not to Dope: The Effect of Sonicating Single-Wall Carbon Nanotubes in Common Laboratory Solvents on their Electronic Structure. *J. Am. Chem. Soc.* **2008**, *130*, 13417–13424.
21. Tummala, N. R.; Striolo, A. SDS Surfactants on Carbon Nanotubes: Aggregate Morphology. *ACS Nano* **2009**, *3*, 595–602.
22. Parra-Vasquez, A. N. G.; Behabtu, N.; Green, M. J.; Pint, C. L.; Young, C. C.; Schmidt, J.; Kesselman, E.; Goyal, A.; Ajayan, P. M.; Cohen, Y.; *et al*. Spontaneous Dissolution of Ultralong Single- and Multiwalled Carbon Nanotubes. *ACS Nano* **2010**, *4*, 3969–3978.
23. Penicaud, A.; Poulin, P.; Derre, A.; Anglaret, E.; Petit, P. Spontaneous Dissolution of a Single-Wall Carbon Nanotube Salt. *J. Am. Chem. Soc.* **2005**, *127*, 8–9.
24. Thompson, J. C. *Electrons in Liquid Ammonia*; Clarendon Press, 1976.
25. Chattopadhyay, J.; Sadana, A. K.; Liang, F.; Beach, J. M.; Xiao, Y.; Hauge, R. H.; Billups, W. E. Carbon Nanotube Salts. Arylation of Single-Wall Carbon Nanotubes. *Org. Lett.* **2005**, *7*, 4067–4069.
26. Liang, F.; Sadana, A. K.; Peera, A.; Chattopadhyay, J.; Gu, Z.; Hauge, R. H.; Billups, W. E. A Convenient Route to Functionalized Carbon Nanotubes. *Nano Lett.* **2004**, *4*, 1257–1260.
27. Pekker, S.; Salvetat, J. P.; Jakab, E.; Bonard, J. M.; Forro, L. Hydrogenation of Carbon Nanotubes and Graphite in Liquid Ammonia. *J. Phys. Chem. B* **2001**, *105*, 7938–7943.
28. Wunderlich, D.; Hauke, F.; Hirsch, A. Preferred Functionalization of Metallic and Small-Diameter Single Walled Carbon Nanotubes via Reductive Alkylation. *J. Mater. Chem.* **2008**, *18*, 1493–1497.
29. Gu, Z.; Liang, F.; Chen, Z.; Sadana, A.; Kittrell, C.; Billups, W. E.; Hauge, R. H.; Smalley, R. E. In Situ Raman Studies on Lithiated Single-Wall Carbon Nanotubes in Liquid Ammonia. *Chem. Phys. Lett.* **2005**, *410*, 467–470.
30. Gebhardt, B.; Graupner, R.; Hauke, F.; Hirsch, A. A Novel Diameter-Selective Functionalization of SWCNTs with Lithium Alkynylides. *Eur. J. Org. Chem.* **2010**, 1494–1501.
31. Zhou, W.; Islam, M. F.; Wang, H.; Ho, D. L.; Yodh, A. G.; Winey, K. I.; Fischer, J. E. Small Angle Neutron Scattering from Single-Wall Carbon Nanotube Suspensions: Evidence for Isolated Rigid Rods and Rod Networks. *Chem. Phys. Lett.* **2004**, *384*, 185–189.
32. Yurekli, K.; Mitchell, C. A.; Krishnamoorti, R. Small-Angle Neutron Scattering from Surfactant-Assisted Aqueous Dispersions of Carbon Nanotubes. *J. Am. Chem. Soc.* **2004** *126*, 9902–9903.
33. Hough, L. A.; Islam, M. F.; Hammouda, B.; Yodh, A. G.; Heiney, P. A. Structure of Semidilute Single-Wall Carbon Nanotube Suspensions and Gels. *Nano Lett.* **2006**, *6*, 313–317.
34. Wang, H.; Zhou, W.; Ho, D. L.; Winey, K. I.; Fischer, J. E.; Glinka, C. J.; Hobbie, E. K. Dispersing Single-Walled Carbon Nanotubes with Surfactants: A Small Angle Neutron Scattering Study. *Nano Lett.* **2004**, *4*, 1789–1793.
35. Howard, C. A.; Thompson, H.; Wasse, J. C.; Skipper, N. T. Formation of Giant Solvation Shells around Fulleride Anions in Liquid Ammonia. *J. Am. Chem. Soc.* **2004**, *126*, 13228–13229.
36. Itkis, M. E.; Perea, D. E.; Niyogi, S.; Rickard, S. M.; Hamon, M. A.; Hu, H.; Zhao, B.; Haddon, R. C. Purity Evaluation of As-Prepared Single-Walled Carbon Nanotube Soot by Use of Solution-Phase Near IR Spectroscopy. *Nano Lett.* **2003**, *3*, 309–314.
37. Tripol'skii, A. I.; T. Serebrii, G.; Lemesh, N. V.; Khavrus', V. A.; Ivashchenko, T. S.; Strizhak, P. E. Fractal Analysis of Carbon Nanotube Agglomerates Obtained by Chemical, Vapor Decomposition of Ethylene over Nickel Nanoparticles. *Theor. Exp Chem.* **2009**, *45*, 103–107.
38. Grigorian, L.; Colbern, S.; Maciel, I. O.; Piamenta, M. A.; Plentz, F.; Jorio, A. Atomic Size-Limited Intercalation into Single Wall Carbon Nanotubes. *Nanotechnology* **2007**, *18*, 435705.
39. Jorio, A.; Fantini, C.; Pimenta, M. A.; Capaz, R. B.; Samsonidze, Ge. G.; Dresselhaus, G.; Dresselhaus, M. S.; Jiang, J.; Kobayashi, N.; Gruneis, A.; Saito, R. Resonance Raman Spectroscopy (n,m)-Dependent Effects in Small-Diameter Single-Wall Carbon Nanotubes. *Phys. Rev. B* **2005**, *71*, 075401.
40. Jorio, A.; Santos, A. P.; Ribeiro, H. B.; Fantini, C.; Souza, M.; Vieira, J. P. M; Furtado, C. A.; Jiang, J.; Saito, R.; Balzano, L.; *et al*.

Quantifying Carbon-Nanotube Species with Resonance Raman Scattering. *Phys. Rev. B* **2005**, *72*, 075207.
41. O'Connell, M. J.; Sivaram, S.; Doorn, S. K. Near-Infrared Resonance Raman Excitation Profile Studies of Single-Walled Carbon Nanotube Intertube Interactions: A Direct Comparison of Bundled and Individually Dispersed HiPco Nanotubes. *Phys. Rev. B* **2004**, *69*, 235415.
42. Paolucci, D.; Franco, M. M.; Iurlo, M.; Marcaccio, M.; Prato, M.; Zerbetto, F.; Penicaud, A.; Paolucci, F. Singling out the Electrochemistry of Individual Single-Walled Carbon Nanotubes in Solution. *J. Am. Chem. Soc.* **2008**, *130*, 7393.
43. Howard, C. A.; Skipper, N. T. Computer Simulations of Fulleride Anions in Metal-Ammonia Solutions. *J. Phys. Chem. B* **2009**, *113*, 3324–3332.
44. Giordani, S.; Bergin, S. D.; Nicolosi, V.; Lebedkin, S.; Kappes, M. M.; Blau, W. J.; Coleman, J. N. Debundling of Single-Walled Nanotubes by Dilution: Observation of Large Populations of Individual Nanotubes in Amide Solvent Dispersions. *J. Phys. Chem. B* **2006**, *110*, 15708–15718.
45. Guan, J.; Martinez-Rubi, Y.; Dénommée, S.; Ruth, D.; Kingston, C. T.; Daroszewska, M.; Barnes, M.; Simard, B. About the Solubility of Reduced SWCNT in DMSO. *Nanotechnology* **2009**, *20*, 245701.
46. Anglaret, E.; Dragin, F.; Pénicaud, A.; Marte, R. Raman Studies of Solutions of Single-Wall Carbon Nanotube Salts. *J. Phys. Chem. B* **2006**, *110*, 3949–3954.
47. Graupner, R.; Abraham, J.; Wunderlich, D.; Vencelová, A.; Lauffer, P.; Röhrl, J.; Hundhausen, M.; Ley, L.; Hirsch, A. Nucleophilic-Alkylation-Reoxidation: A Functionalization Sequence for Single-Wall Carbon Nanotubes. *J. Am. Chem. Soc.* **2006**, *128*, 6683–689.
48. Furtado, C. A.; Kim, U. J.; Gutierrez, H. R.; Pan, L.; Dickey, E. C.; Eklund, P. C. Debundling and Dissolution of Single-Walled Carbon Nanotubes in Amide Solvents. *J. Am. Chem. Soc.* **2004**, *126*, 6095–6105.
49. Voiry, D.; Drummond, C.; Pénicaud, A. Portrait of Carbon Nanotube Salts as Soluble Polyelectrolytes. *Soft Matter* **2011**, *7*, 7998–8001.
50. Kozinsky, B.; Marzari, N. Static Dielectric Properties of Carbon Nanotubes from First Principles. *Phys. Rev. Lett.* **2006**, *96*, 166801.
51. Okazaki, K.; Nakato, Y.; Murakoshi, K. Absolute Potential of the Fermi Level of Isolated Single-Walled Carbon Nanotubes. *Phys. Rev. B* **2003**, *68*, 035434.
52. Hirana, Y.; Tanaka, Y.; Niidome, Y.; Nakashima, N. Strong Micro-Dielectric Environment Effect on the Band Gaps of (n,m) Single-Walled Carbon Nanotubes. *J. Am. Chem. Soc.* **2010**, *132*, 13072–13077.
53. Heenan, R. K. *FISH Data Analysis Program*; Rutherford Appleton Laboratory, Report RAL-89-129; CCLRC: Didcot, UK, **1989**.